



LAWRENCE
LIVERMORE
NATIONAL
LABORATORY

Demonstration of a Three-dimensionally Structured Betavoltaic

J. W. Murphy

July 31, 2020

Journal Of Electronic Materials

Disclaimer

This document was prepared as an account of work sponsored by an agency of the United States government. Neither the United States government nor Lawrence Livermore National Security, LLC, nor any of their employees makes any warranty, expressed or implied, or assumes any legal liability or responsibility for the accuracy, completeness, or usefulness of any information, apparatus, product, or process disclosed, or represents that its use would not infringe privately owned rights. Reference herein to any specific commercial product, process, or service by trade name, trademark, manufacturer, or otherwise does not necessarily constitute or imply its endorsement, recommendation, or favoring by the United States government or Lawrence Livermore National Security, LLC. The views and opinions of authors expressed herein do not necessarily state or reflect those of the United States government or Lawrence Livermore National Security, LLC, and shall not be used for advertising or product endorsement purposes.

Demonstration of a Three-dimensionally Structured Betavoltaic

John W. Murphy^{1*}, Clint D. Frye¹, Roger A. Henderson¹, Mark A. Stoyer¹, Lars F. Voss¹,
Rebecca J. Nikolic^{1*}

¹Lawrence Livermore National Laboratory, 7000 East Ave, Livermore, CA 95440

*Corresponding authors – murphy70@llnl.gov, nikolic1@llnl.gov

Abstract

In this work we present a demonstration of a high-aspect ratio three-dimensionally structured betavoltaic device. High-aspect ratio silicon PIN diodes were used as the semiconductor absorber and $^{147}\text{PmCl}_3$ was used as the beta emitter. Three devices were fabricated with ^{147}Pm activities of 2.4, 7.4, and 29.5 mCi. The device with the highest activity produced an initial power output of 200 nW and was monitored over a period of eight months to observe the current-voltage behavior over time, during which time the output current decreased in accordance with the radioactive half-life of ^{147}Pm . Small deviations in the output current of a few percent during the long-term measurement were found to be attributable to the humidity in the room where the experiment was done. The output current generated from the devices was 68-77% of the theoretical maximum, indicating significant infiltration of the radioisotope into the ridged structures.

Keywords

Betavoltaic, Radioisotope Battery, PIN diode, Nuclear Battery, Promethium, Silicon

Introduction

High-aspect ratio, three-dimensional semiconductor devices have found utility in solid-state neutron detectors [1–4], as well solar cells [5–7], and have been considered for betavoltaic devices as well [8–10]. Betavoltaic devices are electrical power generating current sources that

26 operate by a built-in junction sweeping out the charge produced by the direct ionization of a
27 semiconductor material resulting from beta radiation. They are generally analogous to
28 semiconductor solar cells, except rather than a photon creating an electron-hole pair, each
29 incident beta particle can produce hundreds or thousands of electron-hole pairs. Betavoltaics are
30 a class of nuclear or radioisotope batteries that have been studied since the early 1950s [11,12].
31 As a class of radioisotope batteries, betavoltaics are attractive because they can potentially
32 provide a higher power conversion efficiency compared to other radioisotope-based power
33 sources such as radioisotope thermoelectric generators, particularly for relatively low power
34 outputs of milliwatts or less [13].

35

36 Promethium-based betavoltaics were evaluated for use as a power source for medical implants
37 using planar silicon diodes in the 1970s [14]. These medical implant devices leveraged the
38 pioneering work of Larry Olsen on silicon-based promethium betavoltaic devices [15–17]. More
39 recently wide-bandgap semiconductors such as SiC and GaN have been evaluated for use as
40 betavoltaics [18,19]. However, these wide bandgap materials have less well-developed
41 technology with respect to high-aspect ratio structure and junction formation [20–24]. We have
42 selected silicon for this work as the fabrication of high-aspect ratio three-dimensional PIN
43 diodes, with an aspect ratio up to 40, and conformal junctions that result in low-leakage current
44 over a large area are a technology that has been well-developed [25,26].

45

46 Three-dimensionally structured betavoltaics can potentially offer higher power density and
47 efficiency than traditional co-planar type configurations [10,27]. There have been reports of
48 using porous silicon fabricated by wet-etching for three-dimensional betavoltaics, although to

49 date these devices have suffered from large leakage currents resulting in low output voltage [28–
50 30]. There is a previous report of a design for a three-dimensionally structured betavoltaic based
51 on Si and ^{147}Pm , however the device was only tested using an electron beam from a scanning
52 electron microscope (SEM) [31].

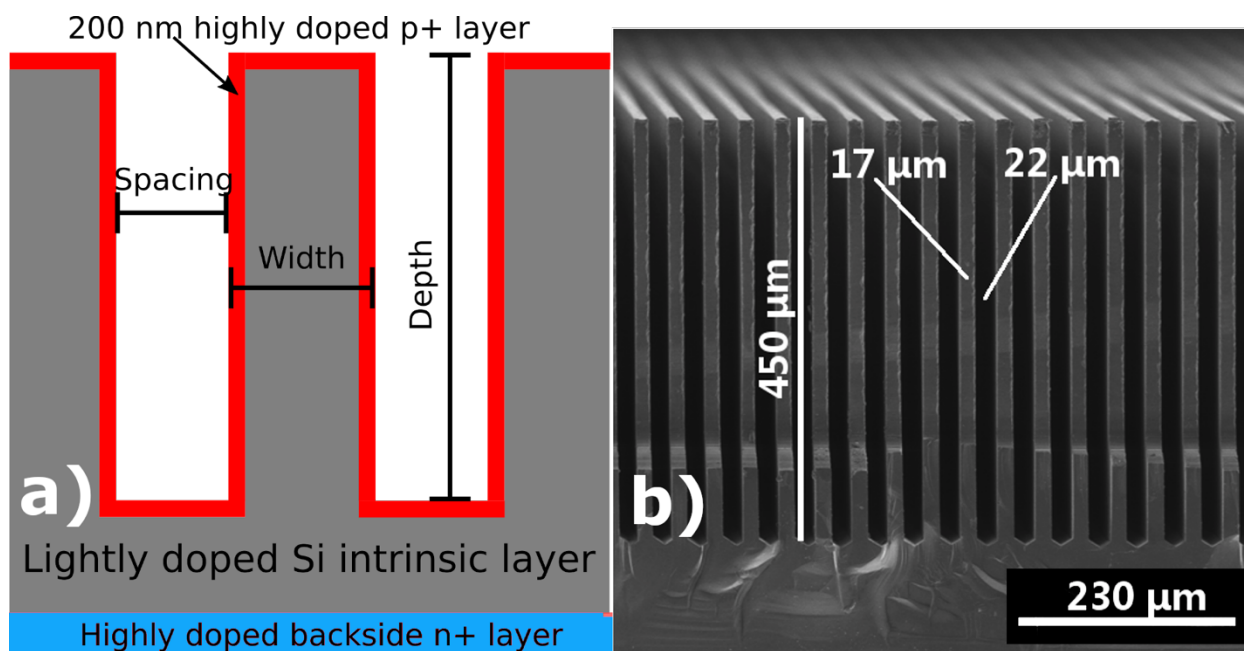
53

54 In this work we fabricated three betavoltaic devices using high-aspect ratio, ridged silicon PIN
55 diodes, and clearly demonstrate infiltration of a promethium radioisotope material into the three-
56 dimensionally structured semiconductor. The space between the ridges in the silicon diodes was
57 filled by dissolving the PmCl_3 source material in an alcohol solution and using a modified drop-
58 casting technique to infiltrate the empty space with radioisotope. The devices were measured
59 over the course of weeks, with measurements of the highest activity device taken for over eight
60 months.

61 Experimental

62 The three PIN diodes used in this work, labeled as Device #1, 2, and 3, were procured from
63 Radiation Detection Technology, Inc. They are ridged silicon structures with a ridge width of
64 $\sim 17\ \mu\text{m}$, a ridge spacing of $\sim 22\ \mu\text{m}$, and a depth of $450\ \mu\text{m}$ with a conformal p+ junction. The
65 ridges are formed by etching the (110) oriented Si wafers in a KOH solution, and the junction is
66 formed by solid-source diffusion of B from a BN source after ridge formation. Each diode is
67 approximately $1 \times 1\ \text{cm}^2$. A schematic of the as-received device and a cross-sectional SEM image
68 are shown in Figure 1. Based on discussions with RDT, Inc. we estimate that the highly-doped
69 p+ region is no thicker than 200 nm. This highly doped p+ layer will effectively be a “dead
70 layer”, as little to no charge that is generated in that region will be collected due to rapid
71 recombination [26].

72



73

74 Figure 1 – (a) Schematic of the ridged Si PIN diodes, and (b) SEM micrograph of a cleaved Si
 75 PIN diode.

76

77 The devices were filled with varying amounts of $^{147}\text{PmCl}_3 \cdot 6(\text{H}_2\text{O})$ by means of a modified drop-

78 casting technique in order to deliver a small aliquot of radioisotope solution across the entire

79 diode chip. The device substrates were first dipped into pure ethanol and then placed face up

80 which resulted in a meniscus of liquid on the top surface of the device contained by surface

81 tension. At this point a small amount of aqueous $^{147}\text{PmCl}_3 \cdot 6(\text{H}_2\text{O})$, 20-40 μl , was pipetted on the

82 ethanol on top of the chip and allowed to mix by diffusion. After the top surface was visibly dry

83 the device was placed on a hot plate at 50 $^\circ\text{C}$ to drive out any remaining ethanol and water from

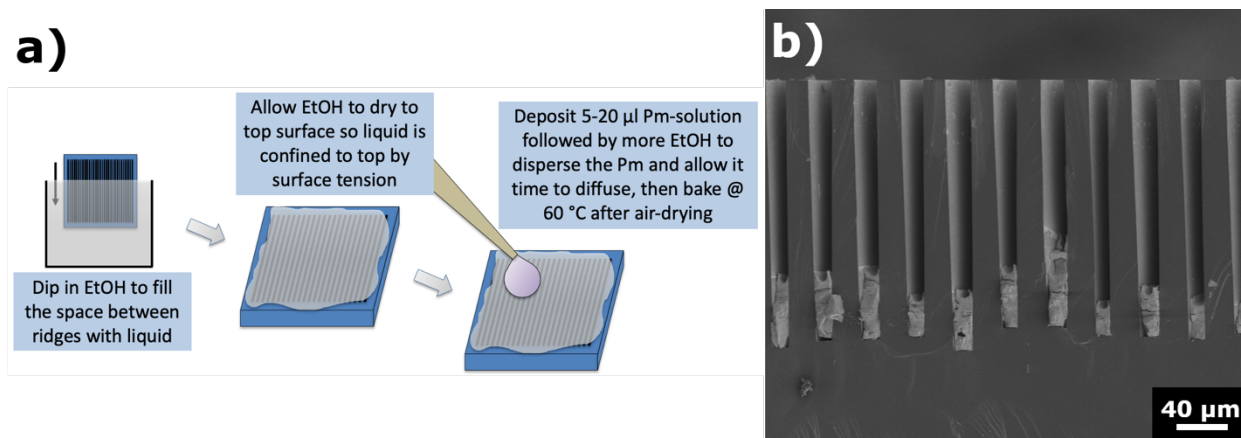
84 inside the ridged regions. A schematic of how this procedure was performed as well as a cross-

85 sectional SEM image of a mock device filled with $\text{NdCl}_3 \cdot 6(\text{H}_2\text{O})$, which was used as a non-

86 radioactive analog material for deposition development and testing, is shown in Figure 2.

87

88



89
 90 Figure 2 – (a) Schematic of the modified drop-casting technique and (b) cross-sectional SEM
 91 image of mock device partially (~15%) filled with NdCl₃·6(H₂O) (lighter regions).
 92
 93 The devices were connected to a ceramic package with graphite paint to make a backside contact
 94 and probed on the contact pad on the top side using a micromanipulator inside of a fume hood.
 95 The I-V curves were recorded using an Agilent 4156B, and the temperature/humidity
 96 measurements were made with a ThorLabs TSP01 temperature and humidity logger with the
 97 probe placed at the front of the hood. The total activity deposited in and on the sample was
 98 determined by gamma counting measurements at the conclusion of I-V testing. The power output
 99 simulations of a fully filled device were carried out in MCNP6 in a manner similar to those
 100 previous reported, accounting for a 200 nm thick highly-doped conformal dead layer [27].

101 Results & Discussion

102 The initial activity, theoretical maximum short-circuit current (I_{SC}), the experimental I_{SC} , the
 103 ratio of these two values, the open-circuit voltage (V_{OC}), fill factor (FF), output power, and
 104 output power density (power normalized by the volume of the semiconductor chip), each at the
 105 start of the experiment, are shown in Table 1. All of the experimental I_{SC} values are within 68-
 106 77% of the theoretical absolute maximum assuming an ionization energy of 3.61 eV per
 107 electron-hole pair – i.e., if no beta particle energy was lost due to a metallic or highly-doped dead
 108 layer between the radioisotope and the active semiconductor region or due to geometrical effects,

109 and all of the energy went towards the generation of electron-hole pairs in the intrinsic region of
 110 the semiconductor. For example, if the radioisotope material was only on the top surface of the
 111 chip, ~50% of the beta particles would be lost due to isotropic emission resulting in an I_{SC} of
 112 approximately one-half of the theoretical maximum I_{SC} [32]. This theoretical max I_{SC} is shown in
 113 Table I along with the experimental I_{SC} at the start of the experiment (immediately following the
 114 radioisotope filling), as well as the ratio of the experimental I_{SC} to the theoretical max I_{SC} . This
 115 ratio being well above 50% indicates that the modified drop-casting technique used in this study
 116 was effective in getting the radioisotope material to infiltrate into the empty volume between the
 117 ridges of the 1 cm² diodes.

118

119 The I-V characteristics of unfilled and filled devices are shown in Figure 3. The unfilled I-V
 120 characteristics of Device #3 are shown in Figure 3a, the leakage current of this device was 8 nA
 121 at a bias of -1 V for an approximately 1 cm² diode. The leakage current is important because
 122 ideally it is equal to the saturation current of the diode, which is inversely related to the open-
 123 circuit voltage of the device when operating. So the lower the leakage current is, the higher the
 124 power output will be due to higher voltage, as shown in equation 1 [33]:

$$125 \quad V_{OC} = n \cdot \frac{kT}{q} \cdot \ln \left(\frac{I_{SC}}{I_0} \right) \quad (1)$$

126 Where V_{OC} is the open-circuit voltage, n is the ideality factor, k is the Boltzmann constant, T is
 127 the temperature in Kelvin, q is the fundamental charge, I_{SC} is the short-circuit current, and I_0 is
 128 the saturation current. Also shown in Figure 3a is the quasi-neutral region saturation current of
 129 the diodes extracted from the y-axis intercept, which is approximately 50 nA [33]. The other
 130 devices displayed very similar unfilled I-V characteristics.

131

132

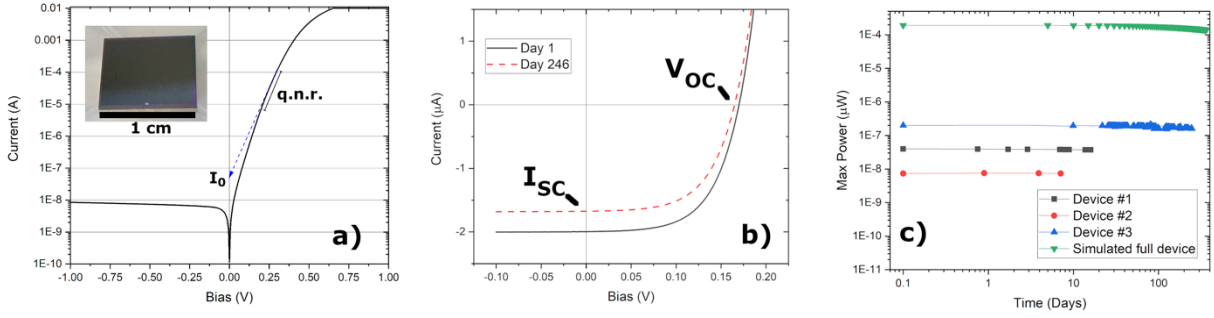
133
134
135
136

Table 1 - Initial activity, theoretical maximum I_{SC} , experimental I_{SC} , ratio of max and experimental I_{SC} , V_{OC} , FF, P_{OUT} , and P_{DEN} at the start of the experiment

Device #	Activity at start (mCi)	Theoretical max I_{SC} at start (μA)	I_{SC} at start (μA)	Ratio of theoretical I_{SC} to exp. I_{SC} (%)	V_{OC} at start (mV)	FF at start (%)	P_{OUT} at start (nW)	P_{DEN} at start ($\mu W/cm^3$)
1	2.4	0.231	0.18	77	90	46	7.4	0.15
2	7.4	0.723	0.54	74	135	55	39.8	0.8
3	29.5	2.932	2.00	68	170	59	200	4

137
138
139
140
141
142
143
144
145
146
147
148
149
150
151
152
153
154
155

The current-voltage (I-V) curves for the filled devices were similar to solar cell output curves, as expected. A labeled output curve from Device #3 is shown in Figure 3b near the start of the test campaign with labels illustrating the relevant metrics mentioned in Table I, including the V_{OC} and I_{SC} . The final I-V curve collected from the device after eight months is also shown. The decrease in I_{SC} for Device #3 generally corresponded to the reduction in activity due to the radioactive decay of ^{147}Pm , albeit with some variation as discussed in the next section. The total power conversion efficiency for Device #3 at the start of the experiment was 1.89%, which is comparable to the value of 2% reported by Olsen et al., during his work on Silicon/Promethium betavoltaics in the late 1960s and early 1970s [34]. It should be noted the efficiency reported by Olsen is for a single planar diode coated with a layer of Pm, meaning that there is geometrical loss of ~50%, so he predicts that the efficiency would be 4% for a sandwich type structure. In this case there is less than 50% geometrical loss due to the 3-dimensional structure, however the short-circuit current is quite low, only 2 μA . A fully-filled diode would have a predicted short-circuit current 0.6 mA, which would increase the open-circuit voltage to nearly 500 mV based on equation 1 and increase the efficiency to a predicted 4.9%. The decay in the power output for all three of the devices over the full period of measurement for each is shown in Figure 3c. Also shown in Figure 3c is the simulated power output over the course of a year for a fully filled device, which would require approximately 11,000 mCi of $^{147}PmCl_3 \cdot 6(H_2O)$.



156
 157 Figure 3 – (a) The I-V curve of Device #3 before filling with a photograph of the device inset,
 158 (b) I-V curve of Device #3 immediately after filling and after eight months, (c) the power output
 159 over the full period of measurement for all three devices as well as the simulated output for a
 160 device that is fully filled with $^{147}\text{PmCl}_3 \cdot 6(\text{H}_2\text{O})$.

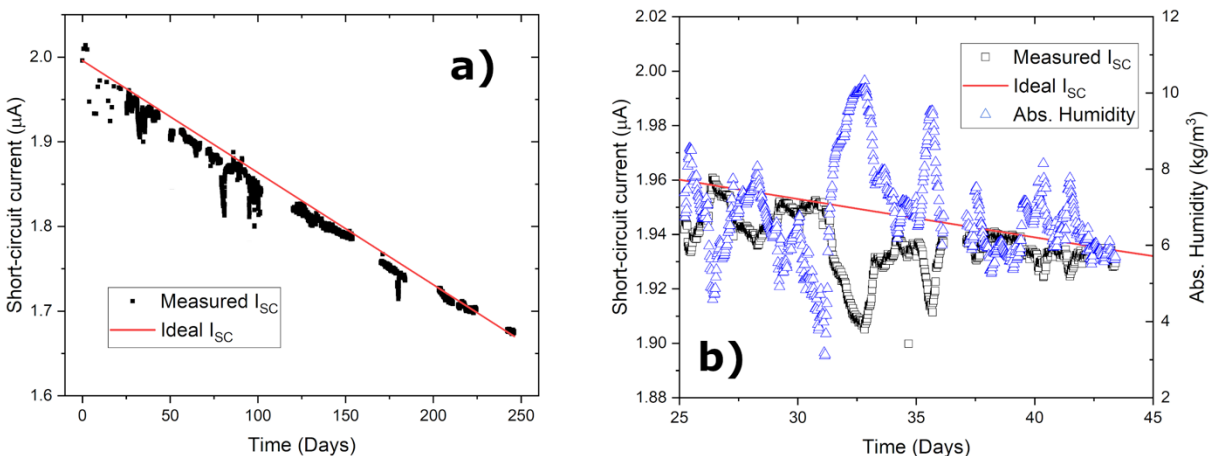
161
 162 The measured I_{SC} of Device #3 over the full duration of the experiment versus the expected
 163 decay in the I_{SC} due to the radioactive decay of the source, marked on the graph as “Ideal I_{SC} ” is
 164 shown in Figure 4a. The short-circuit current decreased from approximately 2 to 1.67 μA , while
 165 the open-circuit voltage declined slightly from 170 to 165 mV (not shown). Based on the
 166 radioactive decay of ^{147}Pm over 246 days we would expect the I_{SC} to decrease from 2 to 1.673
 167 μA , in almost exact agreement with the experimentally observed value. This expected decrease
 168 indicates that there is no excessive degradation to the semiconductor due to deep-level trap
 169 formation from the presence of alpha-emitting radioisotope impurities in the ^{147}Pm material [35].
 170

171 During longer term measurement of Device #3 it was noticed that there was deviation from the
 172 expected decay of the short-circuit current based solely on the decay of ^{147}Pm of a few percent.
 173 To investigate this anomaly a temperature and humidity sensor was placed in front of the fume
 174 hood where the measurements were being taken, and this data was used to calculate the absolute
 175 humidity using the following formula, which is a modified form of the Clausius-Clapeyron
 176 equation [36,37], shown in equation 2:

$$177 \quad H_{\text{abs}} = \frac{6.112 \cdot H_{\text{rel}} \cdot 2.1674 \cdot e^{\frac{17.67 \cdot T}{T+243.5}}}{273.15+T} \quad (2)$$

178

179 Where H_{abs} is the absolute humidity, H_{rel} is the relative humidity, and T is the temperature in
 180 degrees Celsius. It was found that the short-circuit current varied inversely with the absolute
 181 humidity in the room where the measurements were being taken. These results are shown in
 182 Figure 4b for a zoomed-in subsection of the data in Figure 4a, taking only days 25-45 of the
 183 measurement. This can be explained due to the hygroscopic nature of the $\text{PmCl}_3 \cdot 6(\text{H}_2\text{O})$, which
 184 will take up water from the air when the humidity is higher. This additional water in the
 185 radioisotope source material will act to slightly attenuate the beta particle energies on average
 186 before they enter the silicon and generate the charge that will be collected, thus slightly reducing
 187 the current being generated.



188

189 Figure 4 – (a) The short-circuit current over time over the entire measurement period for Device
 190 #3 versus the expected decay based on the half-life of ^{147}Pm , and (b) a zoomed view of the
 191 decline in short-circuit current over time during day 25-45 of measurement plotted against the
 192 absolute humidity showing the correlation between increased humidity and lower short-circuit
 193 current.

194

195 Conclusion

196 We have demonstrated a high-aspect ratio semiconductor betavoltaic device by utilizing ridged
 197 silicon PIN diodes procured from Radiation Detection Technologies, LLC., and $\text{PmCl}_3 \cdot 6(\text{H}_2\text{O})$

198 deposited via a drop-casting technique. The three devices performed as expected, producing
199 between 68-77% of the theoretical maximum short-circuit current, indicating that the majority of
200 the radioisotope material was successfully infiltrated into the volume between the semiconductor
201 ridges. The maximum power produced from a prototype device was initially 200 nW using an
202 activity of 29.5 mCi of ^{147}Pm . This device was measured for over eight months with no
203 appreciable degradation, such as radiation damage, other than what could be attributed to the
204 radioactive decay of the source material. For a device with the architecture used in this study that
205 was fully filled with dense $\text{PmCl}_3 \cdot 6(\text{H}_2\text{O})$ we predict by MCNP6 simulations that the output
206 power would be 192 μW equating to a power density of 3.8 mW/cm^3 . In future work we will
207 develop techniques to completely fill the volume between the ridges with a denser and Pm-rich
208 material such as Pm_2O_3 , optimize the ridge widths and spacing to balance power density and
209 efficiency, and test the long-term reliability of these devices.

210 Acknowledgments

211 We would like to acknowledge Dr. Steve Bellinger and Radiation Detection Technologies LLC
212 for helpful conversations and information. This work was performed under the auspices of the
213 U.S. Department of Energy by Lawrence Livermore National Laboratory under Contract DE-
214 AC52-07NA27344, LLNL-JRNL-813161.

215 Conflict of interest

216 The authors declare that they have no conflict of interest.

217 References

- 218 1. R. J. Nikolic, A. M. Conway, C. E. Reinhardt, R. T. Graff, T. F. Wang, N. Deo, and C. L. Cheung,
219 *Appl. Phys. Lett.* **93**, 133502 (2008).
- 220 2. A. M. Conway, T. F. Wang, N. Deo, C. L. Cheung, and R. J. Nikolic, *IEEE Trans. Nucl. Sci.* **56**,
221 2802 (2009).
- 222 3. S. L. Bellinger, B. W. Cooper, R. G. Fronk, L. C. Henson, T. R. Ochs, T. J. Sobering, and D. S.
223 McGregor, in *IEEE Nucl. Sci. Symp* (2013), pp. 1–7.

- 224 4. J. K. Shultis and D. S. McGregor, *IEEE Trans. Nucl. Sci.* **53**, 1659 (2006).
- 225 5. H. P. Yoon, Y. A. Yuwen, C. E. Kendrick, G. D. Barber, N. J. Podraza, J. M. Redwing, T. E.
- 226 Mallouk, C. R. Wronski, and T. S. Mayer, *Appl. Phys. Lett.* **96**, 213503 (2010).
- 227 6. Y. Lee, H. Kim, S. Q. Hussain, S. Han, N. Balaji, Y.-J. Lee, J. Lee, and J. Yi, *Mater. Sci. Semicond.*
- 228 *Process.* **40**, 391 (2015).
- 229 7. J. R. Maiolo, B. M. Kayes, M. A. Filler, M. C. Putnam, M. D. Kelzenberg, H. A. Atwater, and N.
- 230 S. Lewis, *J. Am. Chem. Soc.* **129**, 12346 (2007).
- 231 8. H. Guo, H. Yang, and Y. Zhang, in *Micro Electro Mech. Syst. 2007. MEMS. IEEE 20th Int. Conf.*
- 232 (2007), pp. 867–870.
- 233 9. K. Zhang, G. Gui, P. Pathak, J.-H. Seo, J. P. Blanchard, and Z. Ma, *Sensors Actuators A Phys.*
- 234 **240**, 131 (2016).
- 235 10. K. Hogan, M. Litz, and F. Shahedipour-Sandvik, *Appl. Radiat. Isot.* **145**, 154 (2019).
- 236 11. W. Ehrenberg, C.-S. Lang, and R. West, *Proc. Phys. Soc. Sect. A* **64**, 424 (1951).
- 237 12. P. Rappaport, *Phys. Rev.* **93**, 246 (1954).
- 238 13. M. Litz, *Isotope Beta-Battery Approaches for Long-Lived Sensors: Technology Review* (2014).
- 239 14. T. H. Smith, J. Greenborg, and W. E. Matheson, *Nucl. Technol.* **26**, 54 (1975).
- 240 15. L. C. Olsen, S. E. Seeman, and B. I. Griffin, *Trans. Am. Nucl. Soc.* **12**, 481 (1969).
- 241 16. L. C. Olsen, *IEEE Trans. Nucl. Sci.* **19**, 375 (1972).
- 242 17. L. C. Olsen, in *Iece* (1974), pp. 754–762.
- 243 18. C. Thomas, S. Portnoff, and M. G. Spencer, *Appl. Phys. Lett.* **108**, 13505 (2016).
- 244 19. M. Litz, *Monte Carlo Evaluation of Tritium Beta Spectrum Energy Deposition in Gallium*
- 245 *Nitride (GaN) Direct Energy Conversion Devices* (2014).
- 246 20. T. Kimoto and J. A. Cooper, *Fundamentals of Silicon Carbide Technology: Growth,*
- 247 *Characterization, Devices and Applications* (John Wiley & Sons, 2014).
- 248 21. C.-C. Tin, S. Mendis, K. Chew, I. Atabaev, T. Saliev, E. Bakhranov, B. Atabaev, V. Adedeji, and
- 249 others, *Thin Solid Films* **518**, e118 (2010).
- 250 22. S. E. Harrison, L. F. Voss, A. M. Torres, C. D. Frye, Q. Shao, and R. J. Nikolić, *J. Vac. Sci.*
- 251 *Technol. A Vacuum, Surfaces, Film.* **35**, 61303 (2017).
- 252 23. M. Sun, Y. Zhang, X. Gao, and T. Palacios, *IEEE Electron Device Lett.* **38**, 509 (2017).
- 253 24. J. Hartmann, F. Steib, H. Zhou, J. Ledig, S. Fündling, F. Albrecht, T. Schimpke, A. Avramescu,
- 254 T. Varghese, H.-H. Wehmann, and others, *Cryst. Growth Des.* **16**, 1458 (2016).
- 255 25. D. S. McGregor and J. Kenneth Shultis, *Nucl. Instruments Methods Phys. Res. Sect. A Accel.*
- 256 *Spectrometers, Detect. Assoc. Equip.* **632**, 167 (2011).
- 257 26. D. S. McGregor, S. L. Bellinger, and J. K. Shultis, *J. Cryst. Growth* **379**, 99 (2013).
- 258 27. J. W. Murphy, L. F. Voss, C. D. Frye, Q. Shao, K. Kazkaz, M. A. Stoyer, R. A. Henderson, and R.
- 259 J. Nikolic, *AIP Adv.* **9**, 65208 (2019).
- 260 28. W. Sun, N. P. Kherani, K. D. Hirschman, L. L. Gadeken, and P. M. Fauchet, *Adv. Mater.* **17**,
- 261 1230 (2005).
- 262 29. J. P. Clarkson, W. Sun, K. D. Hirschman, L. L. Gadeken, and P. M. Fauchet, *Phys. Status Solidi*
- 263 **204**, 1536 (2007).
- 264 30. B. Liu, K. P. Chen, N. P. Kherani, and S. Zukotynski, *Appl. Phys. Lett.* **95**, 233112 (2009).
- 265 31. R. Duggirala, S. Tin, and A. Lal, in *Solid-State Sensors, Actuators Microsystems Conf. 2007.*
- 266 *TRANSDUCERS 2007. Int.* (2007), pp. 279–282.
- 267 32. F. S. Goulding and D. A. Landis, *IEEE Trans. Nucl. Sci.* **29**, 1125 (1982).

- 268 33. D. K. Schroder, *Semiconductor Material and Device Characterization* (John Wiley & Sons,
269 2006).
- 270 34. L. C. Olsen, in *12th Sp. Photovolt. Res. Technol. Conf. (SPRAT 12)* (1993).
- 271 35. H. Flicker, J. J. Loferski, and T. S. Elleman, *IEEE Trans. Electron Devices* **11**, 2 (1964).
- 272 36. J. V Iribarne and W. L. Godson, *Atmospheric Thermodynamics* (Springer Science & Business
273 Media, 2012).
- 274 37. D. Bolton, *Mon. Weather Rev.* **108**, 1046 (1980).
- 275